19 The Temporal Resolution of Functional MRI

P.A. Bandettini

CONTENTS

19.1 Introduction 205
19.1.1 Basics of fMRI Contrast 205
19.1.2 Neuronal-Hemodynamic Cascade of Events 206
19.2 Temporal Resolution Issues 207
19.2.1 Image Acquisition Rate 208
19.2.2 Basic Dynamic Characteristics of the BOLD Signal 208
19.2.3 The Hemodynamic Response to Transient Activation 209
19.2.4 Latency Discernment Within a Voxel or Region of Interest 213
19.2.5 Latency Discernment Across Voxels or Regions of Interest 213
19.3 Increasing the Temporal Resolution 214
19.3.1 Hemodynamic Specificity 215
19.3.2 Neuronal Current Mapping Using NMR Phase Maps? 216
19.4 Conclusions 216
References 217

19.1 Introduction

Since its inception (Bandettini et al. 1992; Frahm et al. 1992; Kwong et al. 1992; Ogawa and Lee 1992), functional MRI (fMRI) has been steadily advancing from a brain activation mapping tool to a means for dynamically assessing brain activation characteristics across time scales ranging from days, to minutes, to tens of milliseconds. Changes in neuronally modulated hemodynamic states across seconds is routinely used to map brain function with fMRI. Changes in the magnitudes and locations of these activated regions over minutes to days with priming, learning, habituation, and reorganization have been studied (Breiter et al. 1996; Buckner et al. 1998a; Buckner and Koutstaal 1998; Cao et al. 1994; Cohen et al. 1997; Karni et al. 1995; Sakai et al. 1998; Schacter and Buckner 1998).

P. A. Bandettini, PhD, Biophysics Research Institute, Medical College of Wisconsin, 8701 Watertown Plank Rd., Milwaukee, WI 53226, USA

Since fMRI contrast is based on hemodynamic changes, the limits of interpretability over any time scale are dependent on the differentiability of neuronally independent hemodynamic changes from neuronally transduced hemodynamic changes. Particularly on the very rapid time scale (milliseconds to seconds), hemodynamic timing variability plays a central role in the limits of fMRI interpretability. It is argued in this chapter that the practical upper limit on functional temporal resolution is determined primarily by the variation of the hemodynamic response latencies in space and in time. To increase the temporal resolution, these variations first need to be better understood.

This chapter is an overview of fMRI temporal resolution. First, the basics of fMRI contrast, as they relate to temporal resolution, are reviewed. Second, fMRI temporal resolution issues are described, and high temporal resolution fMRI strategies are discussed.

19.1.1 Basics of fMRI Contrast

Several types of physiologic information can be mapped using fMRI, including baseline cerebral blood volume (Moonen et al. 1990; Rosen et al. 1989), changes in blood volume (Belliveau et al. 1991), baseline and changes in cerebral perfusion (Detre et al. 1992; Edelman et al. 1994; Kim 1995; Kwong et al. 1994; Williams et al. 1992; Wong et al. 1997, 1998), and changes in blood oxygenation (Bandettini et al. 1992; Frahm et al. 1992; Haacke et al. 1997; Kwong et al. 1992; Ogawa and Lee 1992; Ogawa et al. 1990; Turner et al. 1991). Recently, quantitative measures of the cerebral metabolic rate of oxygen ($CMRO_2$) changes with activation have been derived from fMRI data (Davis et al. 1998; Kim and Ugurbil 1997; van Zijl et al. 1998).

Because of its sensitivity and ease of implementation, the contrast used to observe susceptibility changes with changes in blood oxygenation, coined

blood oxygenation level-dependent (BOLD) contrast by Ogawa et al. (1990), is the most commonly used functional brain imaging contrast used and is the technique that will be primarily discussed in this chapter.

With each of the above-mentioned techniques, the precise type of observable cerebrovascular information can be more finely delineated. Regarding susceptibility contrast imaging, spin-echo sequences are more sensitive to small susceptibility compartments (capillaries and red blood cells) and gradient-echo sequences are sensitive to susceptibility compartments of all sizes (Bandettini and Wong 1995; Boxerman et al. 1995b; Kennan et al. 1994; Ogawa et al. 1993). Outer volume radiofrequency (RF) saturation removes inflowing spins (Duyn et al. 1994), therefore reducing non-susceptibility-related inflow changes when using short TR sequences. Diffusion weighting or "velocity nulling," involving the use of b>50 s^2/mm-reduces the intravascular signal (Boxerman et al. 1995a; Song et al. 1996) therefore reducing, but not eliminating, large vessel effects (intravascular effects are removed but extravascular effects remain) in gradient-echo fMRI and all large vessel effects in spin-echo fMRI. Going to higher field strengths has the same effect as diffusion weighting in the context of susceptibility-based contrast because the T2* and T2 of venous blood become increasingly shorter than the T2* and T2 of gray matter as field strength increases, therefore less signal will arise from within venous blood vessels, at higher field strengths, in sequences having TE=T2 and T2* of gray matter (Menon et al. 1993).

Regarding arterial spin labeling techniques that image perfusion, the time between the inversion "tag" and the image acquisition, the inversion time (TI) roughly determines the predominant vasculature being imaged. A short TI selects rapidly flowing spins (protons in arteries). A long TI selects spins that take longer to reach the imaging plane (protons that are either in capillaries or have exchanged with tissue). Again, as with susceptibility contrast, diffusion weighting gradients reduce or remove intravascular signal in perfusion imaging, allowing the creation of maps that exclusively delineate intravascular capillary and exchanged protons (Wong et al. 1997; Ye et al. 1997). The issues of hemodynamic specificity, in the context of improving temporal resolution, will be discussed in detail in Sect. 19.3.1.

19.1.2 Neuronal-Hemodynamic Cascade of Events

Since fMRI contrast is based on cerebral hemodynamics, to begin to understand the issues in fMRI temporal resolution it is important to have a clear understanding of the cascade of hemodynamic events that follow neuronal activation. After the onset of activation, or rather, after the neuronal firing rate has passed an integrated temporal-spatial threshold, either neuronal, metabolic, or neurotransmitter-mediated signals reach arterial sphincters, causing vessel dilatation. The time for this initial process to occur is likely to be on the order of 100 ms. After vessel dilatation, the blood flow rate increases by 10%–200%, depending on the location and spatial scale of the measurement. The time for blood to travel from arterial sphincters, through the capillary bed to pial veins is thought to be about 2–3 s. This transit time determines when the blood oxygenation saturation increases in each part of the vascular tree.

19.1.2.1 Draining Vein Effects

In the resting state, hemoglobin oxygen saturation is about 95% in arteries and 60% in veins. The increase in hemoglobin saturation with activation is largest in veins, changing in saturation from about 60% to 90%. Likewise, capillary blood oxygen saturation changes from about 80% to 90%. Arterial blood, already saturated, shows practically no change in hemoglobin oxygen saturation. The fact that the largest oxygen saturation change is in veins is one reason why the strongest BOLD effect is usually seen in this part of the vasculature.

The second reason why the strongest BOLD effect is seen in draining veins is that activation-induced BOLD contrast is highly weighted by blood volume in each voxel (Bandettini and Wong 1997b; Boxerman et al. 1995a; Haacke et al. 1995; Jesmanowicz et al., 1998; Kennan et al. 1994; Ogawa et al. 1993; van Zijl et al. 1998). Since capillaries are much smaller than a typical imaging voxel, an extremely large range of voxel volumes in gray matter will likely have a constant 2%–4% capillary blood volume. In contrast, since the size and spacing of draining veins is on the same scale as most imaging voxels, it is likely that veins dominate the relative blood volume in any voxel that they happen to pass through. Voxels that pial veins pass through can have 100% blood volume while voxels that contain no pial

veins may have only 2% blood volume. This stratification in blood volume distribution strongly determines the magnitude stratification of the BOLD signal.

One of the first observations made regarding fMRI signal changes is that after activation, the BOLD signal takes about 2–3 s to begin to deviate from baseline. The time for venous oxygenation to begin to increase appears to be directly correlated to the time that it takes blood to travel from arteries to capillaries and draining veins – about 2–3 s.

19.1.2.2 Blood Volume Change and $CMRO_2$ Change Effects

Other changes, including blood volume dynamics and $CMRO_2$ dynamics relative to flow and oxygenation dynamics, are less well characterized. These relative dynamics are typically invoked to explain other aspects of the BOLD signal change such as the occasionally observed pre-undershoot and the more frequently observed post-undershoot, which represent are essentially decreases in the BOLD signal observed prior to and after the activation-induced signal increase. Evidence exists that blood volume changes are slower than blood flow changes (Mandeville et al. 1998), providing a compelling explanation for the post-undershoot signal. Models constructed to explain the pre-undershoot by blood volume dynamics require a rapid increase of capillary and venous volume (Buxton et al. 1998a, b).

Although no direct measures of rapid $CMRO_2$ changes have been published, the dynamics of $CMRO_2$ changes relative to flow changes have been invoked in the same manner as blood volume dynamics to explain the pre- and post-undershoot in the BOLD contrast signal. The basic hypothesis is that $CMRO_2$ changes happen more rapidly than subsequent flow increases, therefore immediately reducing the saturation of hemoglobin prior to the flow increase that subsequently overcompensates for this effect (Hennig et al. 1995; Hu et al. 1997; Menon et al. 1995a). This hypothesis has been most strongly advocated by laboratories performing optical imaging (Grinvald et al. 1991), since the maps created using this effect show extremely fine detail – suggesting a close proximity to direct metabolic changes and not to secondary hemodynamic effects. The post-undershoot has been explained in a similar manner. Again, the hypothesis is that activation-induced increase in $CMRO_2$ lingers on longer than time for flow to return to a baseline state, therefore reducing the oxygen saturation of hemoglobin until $CMRO_2$ returns to baseline (Frahm et al. 1996).

What matters in the context of temporal resolution is not the time constants or the rapidity of the various activation-induced signal increases and decreases, but the temporal variability of these changes and how accurately these changes can be measured. Figure 19.1 is a representation of the hypothesized approximate onset latency (x axis) and variability (width of shaded regions in x direction) of the cascade of hemodynamic changes that occur following neuronal activation. Also shown are the approximate distance from the neuronal activation source (y axis) and the variability in the distance (width of shaded regions in y direction). The area of the shaded regions give an approximate measure of the spatial and temporal variability. If these areas were reduced to points on a line (i.e., no spatial or temporal variability), then, regardless of the temporal offset and spatial proximity of the hemodynamic event, neuronal activation time and place (the zero intercept) could be precisely determined.

19.2 Temporal Resolution Issues

The temporal resolution of fMRI has been variably defined in the literature. These definitions include the image acquisition rate, the time it takes for the activation-induced response to rise or fall a given

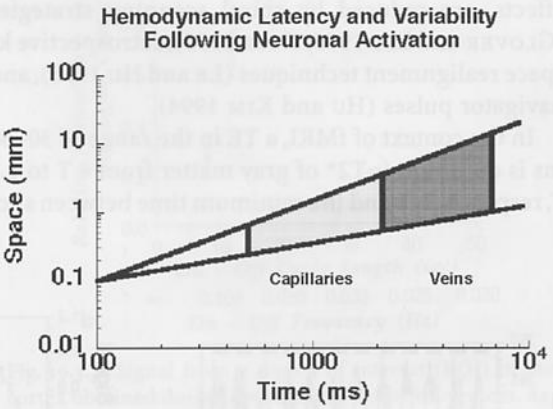

Fig. 19.1. The approximate onset latency (*x axis*) and variability (*width of shaded regions in x direction*) of the hemodynamic changes within capillaries or veins that occur following neuronal activation. Also shown are the approximate distances from the neuronal activation source (*y axis*) and the variability in the distance (*width of shaded regions in y direction*)

amount – otherwise phrased as the time constant of the measured changes, the maximum rate at which activation can be turned on and off and still generate a detectable response, the smallest detectable activation duration, the smallest detectable difference in latency (between two identical activations that have different onset times) in an individual voxel or region of interest (ROI), and the smallest detectable difference in latency across separate voxels or ROIs. Each of these aspects of fMRI temporal resolution are discussed below.

19.2.1 Image Acquisition Rate

The rate at which images are acquired is determined by the choice of pulse sequence. Multi-shot functional imaging techniques, while generally not needing specialized gradient hardware, usually require at least 3 s for image acquisition (Frahm et al. 1993; Glover and Lee 1995; Kim et al. 1993; Noll 1995; Ogawa et al. 1992). A faster technique, single shot echo planar imaging (EPI) (Cohen and Weisskoff 1991; Schmitt et al. 1998; Stehling et al. 1991), generally requires specialized gradients or gradient-switching hardware. The readout window width of an echo planar image is about 20–40 ms. Hybrid techniques such as multi-shot EPI (Butts et al. 1994; McKinnon 1993) provide a good compromise in spatial resolution and time, but suffer from the same shot-to-shot instability as other multi-shot techniques. These instabilities in multi-shot techniques, primarily caused by respiration and cardiac cycle effects, are reduced by spiral scanning strategies (Glover and Lee 1995; Noll 1995), retrospective k-space realignment techniques (Le and Hu 1996), and navigator pulses (Hu and Kim 1994).

In the context of fMRI, a TE in the range of 30–60 ms is optimum (≈T2* of gray matter from 4 T to 1.5 T, respectively), and the minimum time between successive image acquisitions (TR) is typically about 100 ms. With the use of partial k-space acquisition techniques and a shorter and therefore nonoptimal TE, image acquisition rates as high as 60 images per second have been reported (Biswal et al. 1997). Issues regarding the tradeoffs between image acquisition rate and functional contrast have not yet been fully resolved. From a practical standpoint, collection of a multi-slice, whole-brain, volumetric EPI data set requires a TR of about 2 s. The limit of a long TR can be overcome in the context of the cyclic on-off activation time series. Finer temporal sampling of cyclic on-off activation cycle is achievable using a TR that is not an even multiple of the on-off cycle time (Buxton et al. 1998a).

19.2.2 Basic Dynamic Characteristics of the BOLD Signal

Figure 19.2 shows a typical BOLD contrast response from an ROI in motor cortex during repeated cycles of 20 s on, 20 s off finger tapping. Figure 19.2b is the average of the 12 on-off cycles shown in Fig. 19.2a. Several aspects of the BOLD contrast are illustrated here. First, the signal is generally stable over time, although Frahm and colleagues have observed a small drift downward of the baseline and the activation-induced signal change magnitude within the first minutes of either continuous or cyclic on-off visual stimulation (Frahm et al. 1996; Fransson et al. 1998).

With activation, the time for the BOLD response to first significantly increase from baseline is approximately 2 s (DeYoe et al. 1994; Fransson et al. 1998; Kwong et al. 1992). The time to plateau in the on state is approximately 6–9 s (DeYoe et al. 1994). With cessation of activation, the time to return to baseline is longer than the rise time by about 1 or 2 s (Bandettini et al. 1995). As mentioned, several

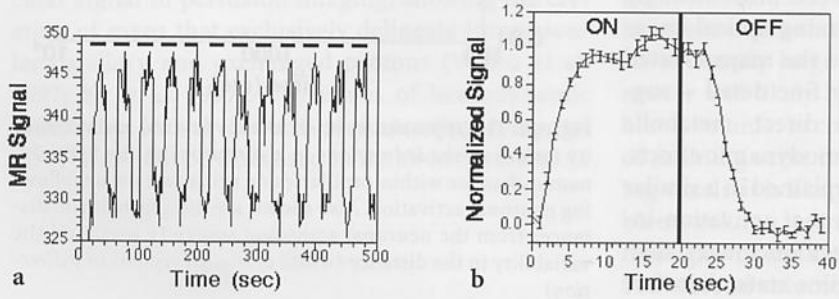

Fig. 19.2. a Typical blood oxygen level-dependent (BOLD) response from a region of interest (ROI) in motor cortex during repeated cycles of 20 s on, 20 s off finger tapping. The time series of echo planar images (EPIs) of the motor cortex were obtained using EPI at 1.5 T. TR=2 s; TE=40 ms. **b** The average of the 12 on-off cycles shown in a

groups have reported a pre-undershoot or initial dip during the first 500 ms (Hennig et al. 1995) to 2 s of the signal (Hu et al. 1997; Menon et al. 1995a). More commonly observed is a post-undershoot, which is observed more in visual cortex than in motor cortex and has an amplitude that is dependent on stimulus duration (Davis et al. 1994). On cessation of activation, the post-undershoot signal can take up to a minute to return to baseline (Bandettini et al. 1997; Fransson et al. 1998).

The hemodynamic response can be thought of as a low-pass filter (Friston et al. 1994). A straightforward method to determine the filter characteristics is to modulate the input and observe the output. Figure 19.3 demonstrates the effect of modulating the on-off motor cortex activation rate from 24 s on, 24 s off to 1 s on, 1 s off. Because the time to reach a baseline after cessation of activity is slightly longer than the time to plateau in an on state, the signal becomes saturated in the on state with the faster on-off frequencies. The relative activation-induced signal amplitude in motor cortex does not show a significant decrease until the switching frequency is higher than 0.06 Hz (8 s on, 8 s off), and does not follow the activation timing above 0.13 Hz. Other work has shown that with sufficient averaging a constant on-off rate of 2 s on, 2 s off is able to induce a measurable hemodynamic response (Bandettini and Cox 1998). Also, the time to reach the saturated on state decreases as the on-off rate increases.

19.2.3 The Hemodynamic Response to Transient Activation

Linear deconvolution of a neuronal input function from the measured hemodynamic response gives a hemodynamic "impulse response" that resembles the type of response that is induced by a brief stimulus – modeled as a Poisson function (Friston et al. 1994) and a γ function (Cohen 1997) among others. The implicit assumption in this analysis is that the hemodynamic response is linear and that the neuronal input is a binary box-car function. Issues related to the linearity of the hemodynamic response become important when considering experimental design and signal interpretability issues and are discussed later in this chapter. Regardless, a brief impulse of activation elicits a response that quite closely resembles the shape of a deconvolved neuronal impulse response. The first "event-related" fMRI experiments were performed using primary

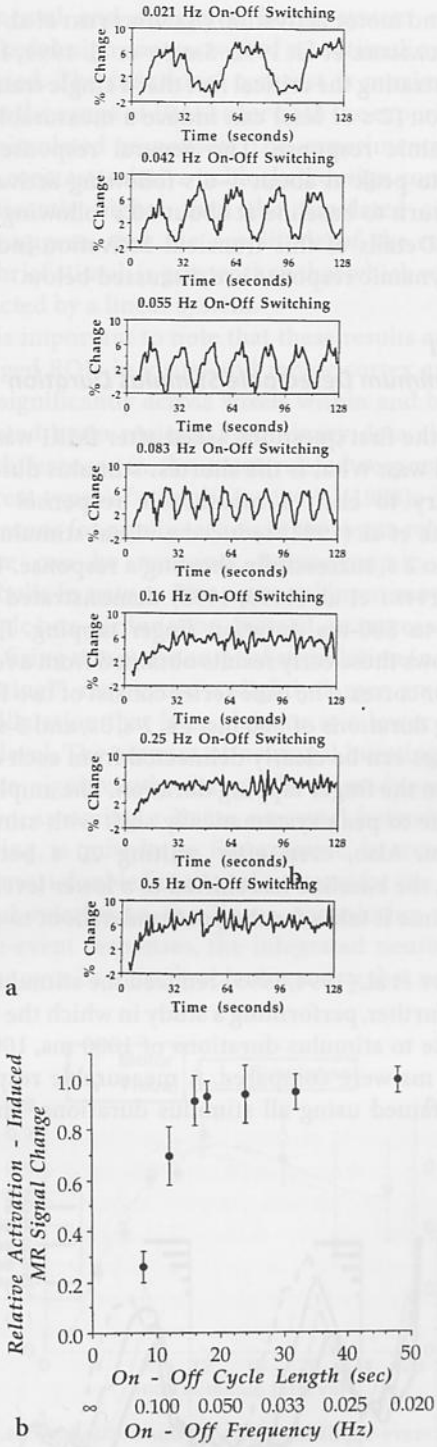

Fig. 19.3. **a** Signal from a region of interest (ROI) in motor cortex obtained during cyclic on/off finger movement. As the on-off frequency is increased from 0.024 Hz to 0.5 Hz, the activation-induced amplitude becomes decreased and the signal becomes saturated in the on state. **b** Summary of the dependence of the relative amplitudes of the activation-induced signal on switching frequency shown in **a**. The relative signal change amplitude is reduced at on-off rates above 0.06 Hz

visual and motor activation (Bandettini et al. 1993, 1995; Blamire et al. 1992; Savoy et al. 1994, 1995), demonstrating the critical fact that a single transient activation (2 s or less) can induce a measurable hemodynamic response. The general response was shown to peak at about 4–6 s following activation, then return to baseline at about 10 s following activation. Details of this transient activation-induced hemodynamic response are discussed below.

19.2.3.1 The Minimum Detectable Stimulus Duration

One of the first questions asked after fMRI was discovered was: What is the shortest stimulus duration necessary to elicit a measurable response? First, Blamire et al. (1992) reduced a visual stimulus duration to 2 s, successfully showing a response. Then, Bandettini et al. (1993, 1995) demonstrated a response to 500-ms duration finger tapping. Figure 19.4 shows these early results obtained from a region in motor cortex. The time series consist of two finger tapping durations of 500 ms, 1 s, 2 s, 3s, and 5 s. The responses czn be clearly delineated from each other based on the finger tapping duration. The amplitude and time to peak systematically shift with stimulus duration. Also, even after waiting 20 s between stimuli, the baseline has shifted to a lower level, due to the time it takes for the post-undershoot to dissipate.

Savoy et al. (1994, 1995) reduced the stimulus duration further, performing a study in which the fMRI response to stimulus durations of 1000 ms, 100 ms, and 34 ms were compared. A measurable response was obtained using all stimulus durations. The responses to the 100 ms and 34 ms stimuli were considerably smaller than the response to the 1000 ms stimulus and were similar in shape and amplitude to each other. These results suggest that the minimum stimulus duration has not yet been determined, but that below a specific stimulus duration, the hemodynamic response remains constant.

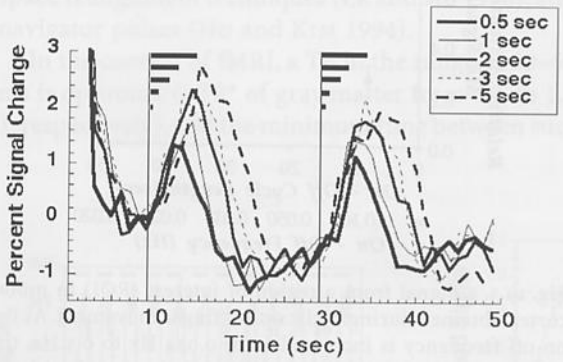

Fig. 19.4. Signal from a region of interest (ROI) in motor cortex across five separate runs during which the subject was cued to perform finger tapping for 0.5, 1, 2, 3, and 5 s twice during the time series. The time between the two finger tapping periods was 20 s; TR=1 s

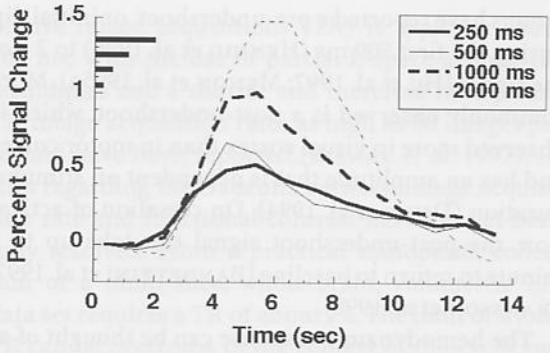

Fig. 19.5. Averaged signal from a region of interest (ROI) in visual cortex across four separate runs during which the subject was given a full field black and white alternating checkerboard stimulus for 250, 500, 1000, and 2000 ms. The total on-off cycle time was 14 s for each stimulus duration. The amplitude and peak time of the response decreases only until 500 ms. The responses to 500 ms and 250 ms stimuli are not significantly different, suggesting a minimum neuronal or hemodynamic activity time of at least 250 ms regardless of the briefness of the input stimulus. TR=1 s

Figure 19.5 demonstrates a similar basic effect as shown by Savoy et al. (1994, 1995), but at longer stimulus durations. Stimulus durations of 250 ms, 500 ms, 1 s, and 2 s were compared. The amplitude and peak time of the response decrease only until 500 ms. The responses to 500 ms and 250 ms stimuli are not significantly different. These data suggest a minimum neuronal or hemodynamic activity time of at least 500 ms regardless of the briefness of the input stimulus.

19.2.3.2 A Paradigm Shift in Experimental Design: Event-Related fMRI

A critical question in event-related fMRI was whether a transient cognitive activation could elicit a significant and usable fMRI signal change. In 1996, Buckner et al. demonstrated that in fact, event-related fMRI lent itself quite well to cognitive activation questions. In their study, a word stem completion task was performed using a "block-design" strategy and an event-related strategy. Robust activation in the regions involved with word generation was observed in both cases.

Given the substantial number of recent publications that use event-related fMRI (Bandettini and Cox, submitted; Birn et al., 1999; Boynton et al. 1996; Buckner et al. 1998a, b; Buckner and Koutstaal 1998; Burock et al. 1998; Clark et al., 1998; Dale and Buckner 1997; Friston et al. 1998a, b; Hennig et al. 1995; Hickok et al. 1997; Josephs et al. 1997; Konishi et al. 1996; Luknowsky et al. 1998; McCarthy et al. 1997; Rosen et al. 1998; Schacter et al. 1997; Zarahn et al. 1997), it is clearly an exciting recent development in fMRI. Several papers describing event-related signal change characteristics and analysis techniques have been recently published (Boynton et al. 1996; Cohen 1997; Dale and Buckner 1997; Friston et al. 1998a; Josephs et al. 1997; Vasquez and Noll 1998).

The advantages of event-related activation strategies are many (Zarahn et al. 1997). These include the ability to more completely randomize task types in a time series, the ability to selectively analyze fMRI response data based on measured behavioral responses to individual trials, and the option to incorporate overt responses into a time series. Separation of motion artifact from BOLD changes is possible by the use of the temporal response differences between motion effects and the BOLD contrast-based changes (Birn et al. 1998).

19.2.3.3 Experimental Design Issues in Event-Related fMRI

Experimental design and interpretation depend on whether the activation-induced hemodynamic response behaves like a linear system. Evidence is currently somewhat conflicting. Boynton et al. (1996) demonstrated that under most circumstances, the hemodynamic response behaves in a linear manner. Nevertheless, they also observed that the amplitude of the response to brief stimuli is larger than a linear system would predict.

This non-linear system observation is supported by Bandettini and Cox (1998). In that study, the optimal interstimulus interval (ISI) was determined and the functional contrast in single event paradigms (2 s stimulus duration) was compared with the contrast of a blocked design (20 s on, 20 s off) paradigm. For comparison, a series of simulated responses were created by linear convolution of the hemodynamic impulse response (Cohen 1997) with a box-car function representing hypothesized underlying neuronal activity. Figure 19.6 shows the experimental and simulated linear system contrast (blocked design contrast=1) of a 2 s stimuli as the ISI is varied. The functional contrast is maximized at ISIs in the range of 10–12 s for both the experimental and simulated responses. The experimentally derived contrast, relative to blocked design contrast, is significantly higher than the simulated contrast. This suggests that the amplitude of the response with brief stimuli is greater than that which would be predicted by a linear system.

It is important to note that these results are from averaged ROIs in visual and motor cortex and may vary significantly across voxels within and between activated brain regions. Preliminary data also suggest differences in the event-related response with different types of stimuli (Janz et al. 1998).

Reasons for nonlinearities in the event-related response can be neuronal, hemodynamic, and/or metabolic in nature. The neuronal input may not be a simple box-car function. Instead, an increased neuronal firing rate at the onset of stimulation (neuronal "bursting") may cause a slightly larger amount of vasodilatation that later plateaus at a lower steady-state level. The amount of neuronal bursting necessary to significantly change the hemodynamic response, assuming a linear neuronal-hemodynamic coupling, is quite large. For example, to account for the almost double functional contrast for the experimental relative to the linear convolution-derived single-event responses, the integrated neuronal response over 2 s must double. Assuming that neuronal

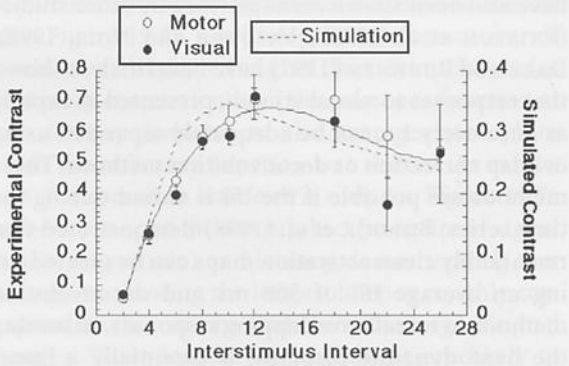

Fig. 19.6. Synthesized and experimental single-event contrast per unit time vs interstimulus interval (ISI). Contrast is normalized to the contrast obtained during the block design time series (blocked design contrast=1). The experimental optimal ISI for a 2 s stimulus duration is shown to be about 12 s. At the optimal ISI, the experimental contrast per unit time is only 35% lower than that of a blocked design paradigm. The synthesized optimal ISI is shown to be about 10 s. At the optimal ISI, the synthesized contrast per unit time is 65% lower than that of a blocked design paradigm

firing is only at a higher rate for about the first 50 ms of brain activation, the neuronal firing rate must be 40 times greater than steady state for this duration.

As is well known, BOLD contrast is highly sensitive to the interplay of blood flow, blood volume, and oxidative metabolic rate. If, with activation, any one of these variables changes with a different time constant, the fMRI signal can show fluctuations until a steady state is reached (Buxton et al. 1998b; Frahm et al. 1996; Menon et al. 1995b). For instance, an activation-induced increase in blood volume would slightly reduce the fMRI signal since more deoxyhemoglobin would be present in the voxel. If the time constant for blood volume changes were slightly longer than that of flow changes, then the activation-induced fMRI signal would first increase then be reduced as blood volume later increased. The same could apply if the time constant of oxidative metabolic rate were slightly slower than that of flow and volume changes. Evidence for increased oxidative metabolic rate after 2 min of activation is given by Frahm et al. (1996), but no evidence suggests that the time constant of the increase in oxidative metabolic rate is only seconds longer than the flow increase time constant – as would be required to be applicable only to relatively high amplitude single- event responses. These hemodynamics, which may also differ on a voxel-wise basis, remain to be characterized fully.

From the above information, it is clear that when using a constant ISI, the optimal ISI is about 10–12 s, and that the response is nonlinear. Nonlinearities have also been shown demonstrated by other studies (Friston et al. 1998b; Vasquez and Noll 1998). Dale and Buckner (1997) have nevertheless shown that responses to visual stimuli, presented as rapidly as once every 1 s, can be adequately separated using overlap correction or deconvolution methods. These methods are possible if the ISI is varied during the time series. Burock et al. (1998) demonstrated that remarkably clean activation maps can be created using an average ISI of 500 ms and deconvolution methods to extract overlapping responses. Assuming the hemodynamic response is essentially a linear system, there is no obvious minimum ISI. Rather, there exists an optimal ISI distribution. As suggested by Dale, an exponential distribution of ISIs, having a mean as short as psychophysically possible, is optimal from a statistical standpoint. Of course the speed with which stimuli can be presented ultimately depends on the study being performed. Many cognitive tasks may require a lower presentation rate. Several cognitive studies have been successfully performed using intermixed, rapidly presented trials (Buckner et al. 1998a; Clark et al., 1998).

While excellent activation maps can be created using rapidly presented stimuli and deconvolution methods, interpretation of details of the deconvolved responses depends on the linearity of the system. Future work in event-related experimental optimization lies in what further information can be derived from these responses. Between-region, between-voxel, between-subject, and stimulus-dependent variations in amplitude, latency, shape, and responsiveness of the event-related fMRI responses are still relatively uncharacterized. The reasons for these differences are also still unclear.

19.2.3.4 Single-Event fMRI: Single Thought Measurement

It should be noted that while individual responses to individual events are easily detectable at low field strengths, the studies described in previous sections involved relatively long time series and considerable averaging or binning of the individual responses into specific categories. These approaches are extremely powerful, but repeatability of individual activation patterns is likely to be somewhat imperfect, especially across trials spaced several minutes apart.

Several recently published studies have demonstrated the ability to create functional maps and to derive useful information using only a single response to a single input. Richter and colleagues have been able to derive the relative onset of activation of supplementary motor cortex relative to primary motor cortex using a delayed motor task following a readiness cue (Kim et al. 1997; Richter et al. 1997a). Also, Richter et al. (1997b) have demonstrated the ability to correlate individual response widths to the duration of a mental rotation task. The larger the angle that an object was mentally rotated the longer the task took and the wider was the event-related parietal region response.

These types of studies represent yet another exciting new direction in fMRI paradigm design. It is imagined that measurement of complex responses from large arrays of cognitive manipulations are achievable in a single time series using this approach. This approach may represent a large jump in one aspect of fMRI temporal resolution – that of usable information per unit time. The combination of single-event fMRI paradigm design with analysis techniques that involve linear regression of multiple expected responses in a single time series (Courtney et al. 1997) may improve even further

the utility of fMRI.

19.2.4 Latency Discernment Within a Voxel or Region of Interest

If a task onset or duration is modulated, such as in the above-mentioned motor cortex tasks or mental rotation studies (Kim et al. 1997; Richter et al. 1997a, b), the accuracy with which one can temporally correlate the modulated input parameters to the measured output signal depends on the variability of the signal within a voxel or region of interest.

Savoy and colleagues (1995) have begun to address this issue of latency estimation accuracy. The variability of several temporal components of an activation-induced response function was determined. Six subjects were studied, and for each subject ten activation-induced response curves were analyzed. The relative onsets were determined by finding the latency with which each of the temporal components was maximized with each of three reference functions, representing three components of the response curve: the entire curve, the rising section, and the falling section. The standard deviations of the entire curve, rising phase, and falling phase were found to be 650 ms, 450 ms, and 1250 ms, respectively. The reasons for the differences between the rising phase and falling phase variability remain unclaer.

19.2.5 Latency Discernment Across Voxels or Regions of Interest

Researchers have reported observing across-region differences in the onset and return to baseline of the BOLD signal during cognitive tasks (Binder et al. 1993; Buckner et al. 1996). For example, during a visually presented, event-related word stem completion task Buckner et al. (1996) reported that the signal in visual cortex increased about 1 s before the signal in the left anterior prefrontal cortex. One might argue that this is expected since the subject first observes the word stem then, after about a second, generates a word to complete this task. Others would argue that the neuronal onset latencies should not be more than about 200 ms. Can inferences of the spatial-temporal cascade characteristics of networked brain activation be made on this time scale from fMRI data? Without controlling for the intrinsic temporal variability of the BOLD signal over space, such inferences cannot be easily made for temporal latency differences below about 4 s. If appropriate controls are performed, then the variability approaches that of a single response in an individual voxel – described in Sect. 19.2.4.

Lee et al. (1995) were the first to observe that the fMRI signal change onset within visual cortex during simple visual stimulation varied from 6 s to 12 s. These latencies were also shown to roughly correlate somewhat with the underlying vascular structure. The earliest onset of the signal change appeared to be in gray matter and the latest onset appeared to occur in the largest draining veins. This basic observation was also made in the motor cortex (Bandettini 1995; Bandettini and Wong 1997c). In one study, latency differences did not show a clear correlation of latency with location of draining veins (Saad et al. 1996).

Figure 19.7 demonstrates three sources of temporal variability. Figure 19.7a is a plot of the average time course from the motor cortex resulting from 2 s finger tapping. The first source of variability is the intrinsic noise in the time series signal. The standard deviation of the signal is on the order of 1%. The second source of variability is that of the hemodynamic response. As mentioned, this ranges from 450 ms to 1250 ms depending on whether one is observing the rising phase of the signal or the falling phase. The third source of variability is the latency spread over space.

The plot in Fig. 19.7a was used as a reference function for correlation analysis and was allowed to shift ±2 s. Figure 19.7b is a histogram of the number of voxels in an activated region that demonstrated a maximum correlation with the reference function at each latency (relative to the average latency) to which the reference function was shifted. As can be seen, the spread in latencies is over 4 s. Figure 19.7c includes a map of the dot product (measure of signal change magnitude) and latency, demonstrating that the regions showing the longest latency roughly correspond to the regions that show the largest signal changes. These largest signal changes are likely to arise from downstream draining veins.

To obtain information about relative onsets of cascaded neuronal activity from latency maps, it is important to characterize the underlying vasculature-related latency distribution at which one is looking. Savoy et al. (1994; Rosen et al. 1998) demonstrated that activation onset latencies of 500 ms were discernible using a visual stimulation timing described as follows. First, the subject viewed a fixa-

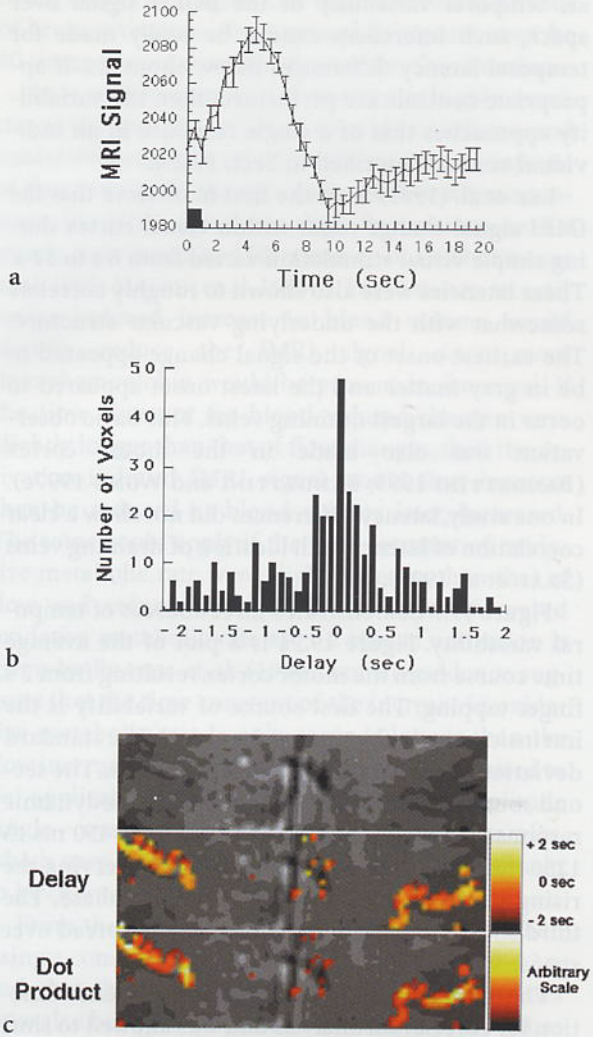

Fig. 19.7a–c. Demonstration of several of the limits of fMRI temporal resolution. Echo planar imaging was performed at 3 Tesla using a Bruker Biospec 3 T/60 equipped with a local head gradient coil. An time course series of axial images (matrix size=96×96, FOV=20 cm, TE=40 ms, TR=500 ms, flip angle=80°) through motor cortex was obtained. Bilateral finger tapping was performed for 2 s, alternating with 18 s rest. The figures demonstrate that the upper temporal resolution is determined by the variability of the signal change in time and space. **a** Time course of the signal elicited by tapping fingers for 2 s. The standard deviation at each point was in the range of 1%–2%. The standard deviation of the hemodynamic change, in time, is in the range of 450–650 ms. **b** Map of the dot product (a measure of the activation-induced signal change magnitude) and the relative latencies or delays of the reference function (the plot in **a** was used as the reference function) at which the correlation coefficient was maximized. The spatial distribution of hemodynamic delays has a standard deviation of about 900 ms. The longest delays approximately match the regions that show the highest dot product and the area where veins are shown as *dark lines* in the T2*-weighted anatomical image. **c** Histogram of relative hemodynamic latencies. This was created from the latency map in **b**

tion point for 10 s. Then, the subject's left visual hemifield was activated 500 ms before the right. Both hemifields were activated for 9 s, then the left hemifield stimulus was turned off 500 ms before the right.

While these onset differences can be shown in a time series derived from an ROI, maps of latency cannot reveal the onset differences because the 4-s variability over space dominates the experimentally inserted 500 ms variability from left to right hemifield. In addition, the onset latency, as derived from a time course obtained from a ROI, is extremely sensitive to the choice in ROI, since the spatial variability is so extreme.

Modulation of the stimulation timing has allowed relative latency differences to be mapped. In the following study, the left-right onset order was switched so that in the first run, the left hemifield was activated and turned off 500 ms and 250 ms prior to the right, and in the second run the right hemifield was activated and turned off 500 ms and 250 ms prior to the left. Latency maps were made for each onset order and subtracted from each other to reveal clear delineations between right and left hemifield that were not apparent in each of the individual maps. This operation is shown in Fig. 19.8. It should be noted that the maps are of the change in onset of one area relative to another and not of absolute latency. Maps such as these may be extremely useful in determining which regions of activation are modulated relative to other areas, given a specific and measurable task timing or response variation.

A similar study by Lukowski et al. (1998) has shown that the mean accuracy of latency measures from multi-voxel ROIs is ±27 ms, which is comparable to that of electrophysiological experiments.

19.3 Increasing the Temporal Resolution

The current upper temporal resolutions of fMRI, and some variables that determine these resolution, as described above, are summarized in Table 19.1. The last estimate in Table 19.1 – that of the range of latencies over space – can be reduced to the standard deviation of the onset time per voxel if the appropriate normalization procedure is performed (as in Sect. 19.2.5) and if only relative latency is desired.

Methods discussed below have potential for increasing the temporal resolution even further. These

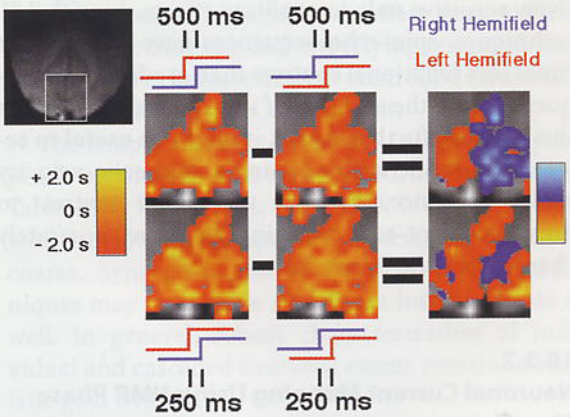

Fig. 19.8. Activation within a region of visual cortex is shown for two separate conditions. In one condition (*left*), the right visual hemifield stimulation precedes the left by 500 ms (*top*) and 250 ms (*bottom*). In the other condition (*middle*), the left precedes the right by 500 ms and 250 ms. Latency maps from both of these conditions show an intrinsic spread of±2.5 s, which is too large to clearly identify the relative latencies across hemifields. However, once the data are normalized for this intrinsic variance by directly comparing the hemodynamic response from the two different lags within individual voxels, the offset between left and right hemifield can be observed (*right*). This is a demonstration that suggests that normalization of the hemodynamic lag can allow small relative temporal offsets to be identified. These normalized offsets can then be compared across regions to make inferences about neuronal delay. For this experiment the TR was 400 ms

Table 19.1. Functional fMRI temporal resolution factors

Temporal resolution factors	Values for each factor
Fastest image acquisition rate	≈64 images/s
Minimum time for signal to significantly deviate from baseline	≈3 s
Fastest on-off rate in which amplitude-is not compromised	≈8 s on, 8 s off
Fastest on-off rate in which hemodynamic response keeps up	≈2 s on, 2 s off
Minimum activation duration	≈30 ms (no limit determined yet, but the response behaves similarly below 500 ms)
Standard deviation of baseline signal	≈1% (less if physiological fluctuations and system instabilities are filtered out)
Standard deviation of onset time estimation	≈450 ms
Standard deviation of return to baseline time estimation	≈1250 ms
Standard deviation of entire on-off response time estimation	≈650 ms
Range of latencies over space	± 2.5 s

include increasing the hemodynamic specificity and the possibility of observation of a non-hemodynamic phenomenon with MRI.

19.3.1 Hemodynamic Specificity

Figure 19.9 shows a stylized depiction of the vascular tree and the corresponding blood transit delay associated with it. Pulse sequence sensitivity is also indicated. As is shown, the hemodynamic sensitivity can be improved by choosing the pulse sequence that is sensitive to the vasculature having the smallest spatial and temporal spread. As suggested by Fig. 19.9, arterial spin labeling (ASL) techniques allow exquisite control over the vasculature that is observed. If the appropriate TI and diffusion weighting are applied, capillary perfusion effects may be selectively observed. Several studies have compared regions of activation between perfusion based sequences and BOLD-based sequences (Bandettini and Wong 1997a, c; Kim and Ugurbil 1997), but none to date have compared the latency ranges in regions demonstrating perfusion changes with voxels showing only BOLD changes. It is hypothesized that such a study would reveal that the distribution of latencies across voxels showing perfusion changes (because of the capillary specificity) would be smaller than the distribution of latencies across voxels showing BOLD changes.

A practical issue is that ASL techniques, while having more selective sensitivity to capillary effects, have about two to four times less sensitivity. Also, because of the long TI necessary and because pairs of sequentially obtained images are collected, the time between acquisition of each image is long (≈4 s), making any temporal sampling prohibitively coarse. One way around this temporal sampling problem is by having the on-off cycle rate not be divided evenly by the image acquisition rate, therefore each on-off cycle will be sampled at a slightly different time.

Alternatively, if high contrast to noise and short temporal spacing are necessary, perhaps ASL may be used in the identification of voxels showing only

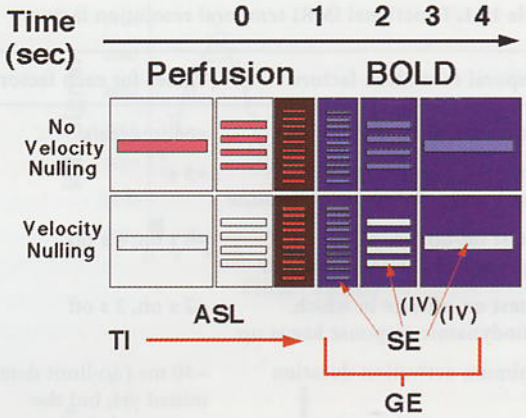

Fig. 19.9. The vascular tree, including arteries (*left*), arterioles, capillaries, and veins (*right*). If the inside of the vessel is filled in, the signal is arising from intravascular spins. Arterial spin labeling (*ASL*) is differentially sensitive to the arterial-capillary region of the vasculature, depending on the TI used and whether or not velocity nulling (diffusion weighting) gradients are used. A small amount of velocity nulling and a TI of about 1 s makes ASL techniques selectively sensitive to capillaries. Susceptibility-based techniques, including gradient-echo (*GE*) and spin-echo (*SE*), are also differentially sensitive to specific aspects of the vasculature. GE techniques are sensitive to susceptibility perturbers of all sizes, therefore they are sensitive to all intravascular and extravascular effects. SE techniques are sensitive to susceptibility perturbers about the size of a red blood cell or capillary, making them sensitive to intravascular (*IV*) effects in vessels of all sizes and to extravascular capillary effects. Velocity nulling makes GE sequences sensitive to extravascular capillary to vein effects, and makes SE sequences selectively sensitive to only capillary effects

capillary effects; then gradient-echo sequences with shorter TR values may be used to observe the signal change dynamics from these voxels.

Susceptibility-based techniques have different vascular sensitivities and therefore different temporal accuracy, depending on the vasculature. Gradient-echo techniques are sensitive to susceptibility perturbers of all sizes, and therefore sensitive to all intravascular and extravascular effects. Interestingly, (multi-shot) gradient-echo techniques that use short TR may be more sensitive to inflow effects which mostly happen upstream in arteries. The onset of these effects may be earlier than those observed using capillary-based contrast. Spin-echo techniques are sensitive to susceptibility perturbers about the size of a red blood cell or capillary, causing them to be sensitive to intravascular effects in vessels of all sizes and to extravascular capillary effects. Velocity nulling causes gradient-echo sequences to be sensitive to only extravascular effects (from capillaries to veins), and causes spin-echo sequences to be selectively sensitive only to capillary effects. As with ASL techniques, spin-echo sequences have two to four times less functional contrast than gradient-echo sequences, and the addition of velocity nulling reduces this contrast further. Again, it might be useful to select the specific regions using a spin-echo velocity nulled sequence, then use the higher contrast to noise gradient-echo imaging to more accurately characterize the dynamics.

19.3.2 Neuronal Current Mapping Using NMR Phase Maps?

As discussed extensively in this chapter, the temporal resolution of fMRI is limited by the variability of the hemodynamic response. A question that most fMRI developers have probably asked themselves is: Are there any other MRI-measurable signatures of brain activation that allow more precise temporal and spatial accuracy? One phenomenon that is, by most calculations, likely to be too small by at least an order of magnitude is magnetic field changes caused by coherent neuronal currents in the brain. These electrical currents and magnetic fields are measured at the scalp using electroencephalography (EEG) and magnetoencelography (MEG), respectively. The hypothesis is that these currents may be measurable at their source, using changes in NMR phase-sensitive to subtle coherent B_0 shifts. A recent abstract has demonstrated that currents on the order of 10 μA are detectable (Li et al. 1998). A useable map of brain function using this technique remains to be seen. Nevertheless, the hope of obtaining images of the brain having the spatial resolution of MRI and the temporal resolution of MEG is extremely motivating.

19.4 Conclusions

As of June 1998, fMRI temporal resolution remains a moving target as it is changing at a rate that is so fast that any characterization becomes obsolete within a short time. New results, providing new hopes or new reasons for caution, are being rapidly published. It has hopefully been made clear in the chapter that the upper temporal resolution of fMRI depends not only on how well we understand neuronal-hemodynamic coupling, but also on how robustly the spa-

tially dependent variables that affect neuronal-hemodynamic coupling and underlying temporal variability can be characterized or controlled on a voxel-wise basis during each experiment.

The temporal resolution of fMRI also strongly depends on the question being asked, as illustrated in Table 19.1. For specific questions, it compares well with the fastest techniques. For others, it is extremely coarse. Synergistic use of fMRI with other techniques may precipitate significant improvements as well. In general, robust characterization of individual and cascaded neuronal events remains a realistic goal with fMRI.

Acknowledgments. This work was supported by the National Institute of Mental Health grant MH51358. Ted DeYoe, Ph.D. and Ziad Saad were critical in obtaining the results shown in Fig. 19.5. Many of the elements of this chapter were brought together as a result of an ongoing lecture given by the author at the MGH visiting fellowship fMRI course, organized by Robert Savoy, Ph.D.

References

Bandettini PA (1995) Magnetic resonance imaging of human brain activation using endogenous susceptibility contrast. PhD dissertation, Biophysics Research Institute, Medical College of Wisconsin, Milwaukee

Bandettini PA, Cox RW (1998) Contrast in single-trial fMRI: interstimulus interval dependency and comparison with blocked strategies. In: Proc ISMRM 6th Annu Meeting, Sydney, p.161

Bandettini PA, Cox RW Functional contrast in event-related fMRI: theory and experiment. Hum Brain Mapp (submitted)

Bandettini PA, Wong EC (1995) Effects of biophysical and physiologic parameters on brain activation-induced R2* and R2 changes: simulations using a deterministic diffusion model. Int J Imag Syst Technol 6:134–152

Bandettini PA, Wong EC (1997a) Analysis of embedded-contrast fMRI: interleaved perfusion, BOLD, and velocity nulling. In: Proc ISMRM 5th Annu Meeting, Vancouver, p.156

Bandettini PA, Wong EC (1997b) A hypercapnia-based normalization method for improved spatial localization of human brain activation with fMRI. NMR Biomed 10:197–203

Bandettini PA, Wong EC (1997c) Magnetic resonance imaging of human brain function: principles, practicalities, and possibilities. Neurosurg Clin North Am 8:345–371

Bandettini PA, Wong EC, Hinks RS, Tikofsky RS, Hyde JS (1992) Time course EPI of human brain function during task activation. Magn Reson Med 25:390–397

Bandettini PA, Wong EC, DeYoe EA, Binder JR, Rao SM, Birzer D et al. (1993) The functional dynamics of blood oxygenlevel dependent contrast in the motor cortex. In: Proc SMRM 12th Annu Meeting. New York, p.1382

Bandettini PA, Wong EC, Binder JR, Rao SM, Jesmanowicz A, Aaron EA et al. (1995) Functional MRI using the BOLD approach: dynamic characteristics and data analysis methods. In: LeBihan D (ed) Diffusion and perfusion: magnetic resonance imaging. Raven, New York, pp 335–349

Bandettini PA, Kwong KK, Davis TL, Tootell RBH, Wong EC, Fox PT et al. (1997) Characterization of cerebral blood oxygenation and flow changes during prolonged brain activation. Hum Brain Mapp 5:93–109

Belliveau JW, Kennedy DN, McKinstry RC, Buchbinder BR, Weisskoff RM, Cohen MS et al. (1991) Functional mapping of the human visual cortex by magnetic resonance imaging. Science 254:716–719

Binder JR, Jesmanowicz A, Rao SM, Bandettini PA, Hammeke TA, Hyde JS (1993) Analysis of phase differences in periodic functional MRI activation data. In: Proc SMRM 12th Annu Meeting, New York, p.1383

Birn RM, Bandettini PA, Cox RW, Shaker R (1998) FMRI during stimulus correlated motion and overt subject responses using a single trial paradigm. In: Proc ISMRM 6th Annu Meeting, Sydney, p.159

Birn RM, Bandettini PA, Cox RW, Shaker R (1999) Event-related fMRI of tasks involving brief motion. Hum Brain Mapp 7:106-114

Biswal B, Jesmanowicz A, Hyde JS (1997) High temporal resolution FMRI. In: Proc ISMRM 5th Annu Meeting, Vancouver, p. 1629

Blamire AM, Ogawa S, Ugurbil K, Baker JR, Davis TL, Rosen BR, Rothman D, McCarthy G, Ellermann JM et al. (1992) Dynamic mapping of the human visual cortex by high-speed magnetic resonance imaging. Proc Natl Acad Sci USA 89:11069–11073

Boxerman JL, Bandettini PA, Kwong KK, Baker JR, Davis TL, Rosen BR et al. (1995a) The intravascular contribution to fMRI signal change: Monte Carlo modeling and diffusion-weighted studies in vivo. Magn Reson Med 34:4–10

Boxerman JL, Hamberg LM, Rosen BR, Weisskoff RM (1995b) MR contrast due to intravascular magnetic susceptibility perturbations. Magn Reson Med 34:555–566

Boynton GM, Engel SA, Glover GH, Heeger DJ (1996) Linear systems analysis of functional magnetic resonance imaging in human V1. J Neurosci 16:4207–4221

Breiter HC, Etcoff NL, Whalen PJ, Kennedy WA, Rauch SL, Buckner RL et al. (1996) Response and habituation of the human amygdala during visual processing of facial expression. Neuron 17:875–887

Buckner RL, Koutstaal W (1998) Functional neuroimaging studies of encoding, priming, and explicit memory retrieval. Proc Natl Acad Sci USA 95:891–898

Buckner RL, Bandettini PA, O'Craven KM, Savoy RL, Peterson SE, Raichle ME et al. (1996) Detection of cortical activation during averaged single trials of a cognitive task using functional magnetic resonance imaging. Proc Natl Acad Sci USA 93:14878–14883

Buckner RL, Goodman J, Burock M, Rotte M, Koutstaal W, Schacter D et al. (1998a) Functional-anatomic correlates of object priming in humans revealed by rapid presentation event-related fMRI. Neuron 20:285–296

Buckner RL, Koutstaal W, Schacter DL, Wagner AD, Rosen BR (1998b) Functional-anatomic study of episodic retrieval using fMRI. Neuroimage 7:151–162

Burock MA, Buckner RL, Dale AM (1998) Understanding differential responses in event related fMRI through linear simulation. In: Proc ISMRM 6th Annu Meeting, Sydney, p. 245

Butts K, Riederer SJ, Ehman RL, Thompson RM, Jack CR (1994) Interleaved echo planar imaging on a standard MRI system. Magn Reson Med 31:67–72

Buxton RB, Luh WM, Wong EC, Frank LR, Bandettini PA (1998a) Diffusion-weighting attenuates the BOLD signal change but not the post-stimulus undershoot. In: Proc ISMRM 6th Annu Meeting, Sydney, p. 7

Buxton RB, Wong EC, Frank LR (1998b) Dynamics of blood flow and oxygenation changes during brain activation: the balloon model. Magn Reson Med 39:855–864

Cao Y, Vikingstad EM, Huttenlocher PR, Levin DN (1994) Functional magnetic resonance studies of the reorganization of the human hand sensorimotor area after unilateral brain injury in the perinatal period. Proc Natl Acad Sci USA 91:9612–9616

Clark VP, Maisog JM, Haxby JV (1998) fMRI study of face perception and memory using random stimulus sequences. J Neurophys 79:3257–3265

Cohen JD, Perlstein WM, Braver TS, Nystrom LE, Noll DC, Jonides J et al. (1997) Temporal dynamics of brain activation during a working memory task. Nature 386:604–607

Cohen MS (1997) Parametric analysis of fMRI data using linear systems methods. Neuroimage 6:93–103

Cohen MS, Weisskoff RM (1991) Ultra-fast imaging. Magn Reson Imaging 9:1–37

Courtney SM, Ungerleider LG, Keil K, Haxby JV (1997) Transient and sustained activity in a distributed neural system for human working memory. Nature 386:608–611

Dale AM, Buckner RL (1997) Selective averaging of rapidly presented individual trials using fMRI. Hum Brain Mapp 5:329–340

Davis TL, Weisskoff RM, Kwong KK, Savoy R, Rosen BR (1994) Susceptibility contrast undershoot is not matched by inflow contrast undershoot. In: Proc SMR 2nd Annu Meeting, San Francisco

Davis TL, Kwong KK, Weisskoff RM, Rosen BR (1998) Calibrated functional MRI: mpping the dynamics of oxidative metabolism. Proc Natl Acad Sci USA 95:1834–1839

Detre JA, Leigh JS, WIlliams DS, Koretsky AP (1992) Perfusion imaging. Magn Reson Med 23:37–45

DeYoe EA, Bandettini P, Neitz J, Miller D, Winans P (1994) Functional magnetic resonance imaging (FMRI) of the human brain. J Neurosci Methods 54:171–187

Duyn JH, Moonen CTW, vanYperen GH, de Boer RW, Luyten PR (1994) Inflow versus deoxyhemoglobin effects in BOLD functional MRI using gradient-echoes at 1.5 T. NMR Biomed 7:83–88

Edelman RR, Sievert B, Wielopolski P, Pearlman J, Warach S (1994) Noninvasive mapping of cerebral perfusion by using EPISTAR MR angiography. J Magn Reson Imaging 4(P):68 (abstract)

Frahm J, Bruhn H, Merboldt K-D, Hanicke W, Math D (1992) Dynamic MR imaging of human brain oxygenation during rest and photic stimulation. J Magn Reson Imaging 2:501–505

Frahm J, Merboldt K-D, Hanicke W (1993) Functional MRI of human brain activation at high spatial resolution. Magn Reson Med 29:139–144

Frahm J, Krüger G, Merboldt K-D, Kleinschmidt A (1996) Dynamic uncoupling and recoupling of perfusion and oxidative metabolism during focal activaiton in man. Magn Reson Med 35:143–148

Fransson P, Krüger G, Merboldt K-D, Frahm J (1998) Temporal characteristics of oxygenation-sensitive responses to visual activation in humans. Magn Reson Med 39:912–919

Friston KJ, Jezzard P, Turner R (1994) Analysis of functional MRI time-series. Hum Brain Mapp 2:69–78

Friston KJ, Fletcher P, Josephs O, Holmes A, Rugg MD, Turner R (1998a) Event-related fMRI: characterizing differential responses. Neuroimage 7:30–40

Friston KJ, Josephs O, Rees G, Turner R (1998b) Nonlinear event-related responses in fMRI. Magn Reson Med 39:41–52

Glover GH, Lee AT (1995) Motion artifacts in fMRI: comparison of 2DFT with PR and spiral scan methods. Magn Reson Med 33:624–635

Grinvald A, Frostig RD, Siegel RM, Bratfeld E (1991) High-resolution optical imaging of functional brain architecture in the awake monkey. Proc Natl Acad Sci USA 88:11559–11563

Haacke EM, Lai S, Yablonski DA, Lin W (1995) In vivo validation of the BOLD mechanism: a review of signal changes in gradient-echo functional MRI in the presence of flow. Int J Imag Syst Technol 6:153–163

Haacke EM, Lai S, Reichenbach JR, Kuppusamy K, Hoogenraad FGC, Takeichi H et al. (1997) In vivo measurement of blood oxygen saturation using magnetic resonance imaging: a direct validation of the blood oxygen level-dependent concept in functional brain imaging. Hum Brain Mapp 5:341–346

Hennig J, Janz C, Speck O, Ernst T (1995) Functional spectroscopy of brain activation following a single light pulse: examinations of the mechanism of the fast initial response. Int J Imag Syst Technol 6:203–208

Hickok G, Love T, Swinney D, Wong EC, Buxton RB (1997) Functional MR imaging during auditory word perception: a single-trial presentation paradigm. Brain Language 58: 197–201

Hu X, Kim S-G (1994) Reduction of signal fluctuations in functional MRI using navigator echoes. Magn Reson Med 31:495–503

Hu X, Le TH, Ugurbil K (1997) Evaluation of the early response in fMRI in individual subjects using short stimulus duration. Magn Reson Med 37:877–884

Janz C, Schmitt C, Fischer H, Speck O, Hennig J (1998) Variability of the hemodynamic response to different stimuli in single event paradigms. In: Proc ISMRM 6th Annu Meeting, Sydney

Jesmanowicz A, Bandettini PA, Hyde JS (1998) Single-shot half k-space high-resolution gradient-recalled EPI for fMRI at 3 tesla. Magn Reson Med 40:754-762

Josephs O, Turner R, Friston K (1997) Event-related fMRI. Hum Brain Mapp 5:243–248

Karni A, Meyer G, Jezzard P, Adams MM, Turner R, Ungerleider LG (1995) Functional MRI evidence for adult motor cortex plasticity during motor skill learning. Nature 377:155–158

Kennan RP, Zhong J, Gore JC (1994) Intravascular susceptibility contrast mechanisms in tissues. Magn Reson Med 31:9–21

Kim S-G (1995) Quantification of relative cerebral blood flow change by flow-sensitive alternating inversion recovery

(FAIR) technique: application to functional mapping. Magn Reson Med 34:293–301

Kim S-G, Ugurbil K (1997) Comparison of blood oxygenation and cerebral blood flow effects in fMRI: estimation of relative oxygen consumption change. Magn Reson Med 38:59–65

Kim S-G, Ashe J, Georgopoulos AP, Merkle H, Ellermann JM, Menon RS (1993) Functional imaging of human motor cortex at high magnetic field. J Neurophysiol 69:297–302

Kim S-G, Richter W, Ugurbil K (1997) Limitations of temporal resolution in fucntional MRI. Magn Reson Med 37:631–636

Konishi S, Yoneyama R, Itagaki H, Uchida I, Nakajima K, Kato H et al. (1996) Transient brain activity used in magnetic resonance imaging to detect functional areas. Neuroreport 8: 19–23

Kwong KK, Belliveau JW, Chesler DA, Goldberg IE, Weisskoff RM, Poncelet BP et al. (1992) Dynamic magnetic resonance imaging of human brain activity during primary sensory stimulation. Proc Natl Acad Sci USA 89:5675–5679

Kwong KK, Chesler DA, Weisskoff RM, Rosen BR (1994) Perfusion MR imaging. In: Proc SMR 2nd Annu Meeting, San Francisco

Le TH, Hu X (1996) Retrospective estimation and correction of physiological artifacts in fMRI by direct extraction of physiological activity form MR data. Magn Reson Med 35:290–298

Lee AT, Glover GH, Meyer CH (1995) Discrimination of large venous vessels in time-course spiral blood-oxygen-level-dependent magnetic-resonance functional neuroimaging. Magn Reson Med 33:745–754

Li S-J, Jesmanowicz A, Bodurka J, Hyde J (1998) Current-induced magnetic resonance phase imaging. In: Proc ISMRM 6th Annu Meeting, Sydney, p.1495

Luknowsky DC, Gati JS, Menon RS (1998a) Mental chronometry using single trials and EPI at 4 T. In: Proc ISMRM 6th Annu Meeting, Sydney, p.167

Mandeville JB, Marota JJA, Kosofky BE, Keltner JR, Weissleder R, Rosen BR et al. (1998) Dynamic functional imaging of relative cerebral blood volume during rat forepaw stimulation. Magn Reson Med 39:615–624

McCarthy G, Luby M, Gore J, Goldman-Rakic P (1997) Infrequent events transiently activate human prefrontal and parietal cortex as measured by functional MRI. J Neurophysiol 77:1630–1634

McKinnon GC (1993) Ultrafast interleaved gradient-echo-planar imaging on a standard scanner. Magn Reson Med 30:609–616

Menon RS, Ogawa S, Tank DW, Ugurbil K (1993) 4 Tesla gradient recalled echo characteristics of photic stimulation-induced signal changes in the human primary visual cortex. Magn Reson Med 30:380–386

Menon RS, Ogawa S, Strupp JP, Anderson P, Ugurbil K (1995a) BOLD based functional MRI at 4 tesla includes a capillary bed contribution: echo-planar imaging correlates with previous optical imaging using intrinsic signals. Magn Reson Med 33:453–459

Menon RS, Ogawa S, Ugurbil K (1995b) High-temporal-resolution studies of the human primary visual cortex at 4 T: teasing out the oxygenation contribution in FMRI. Int J Imag Syst Technol 6:209–215

Moonen CTW, van Zijl PCM, Frank JA, LeBihan D, Becker ED (1990) Functional magnetic resonance imaging in medicine and physiology. Science 250:53–61

Noll DC (1995) Methodologic considerations for spiral k-space functional MRI. Int J Imag Syst Technol 6:175–183

Ogawa S, Lee TM (1992) Functional brain imaging with physiologically sensitive image signals. J Magn Reson Imaging 2(P)-WIP (Suppl):S22 (abstract)

Ogawa S, Lee TM, Kay AR, Tank DW (1990) Brain magnetic resonance imaging with contrast dependent on blood oxygenation. Proc Natl Acad Sci USA 87:9868–9872

Ogawa S, Tank DW, Menon R, Ellermann JM, Kim S-G, Merkle H et al. (1992) Intrinsic signal changes accompanying sensory stimulation: functional brain mapping with magnetic resonance imaging. Proc Natl Acad Sci USA 89:5951–5955

Ogawa S, Menon RS, Tank DW, Kim S-G, Merkle H, Ellerman JM et al. (1993) Functional brain mapping by blood oxygenation level-dependent contrast magnetic resonance imaging: a comparison of signal characteristics with a biophysical model. Biophys J 64:803–812

Richter W, Andersen PM, Georgopolous AP, Kim S-G (1997a) Sequential activity in human motor areas during a delayed cued finger movement task studied by time-resolved fMRI. Neuroreport 8:1257–1261

Richter W, Ugurbil K, Georgopouloos A, Kim S-G (1997b) Time-resolved fMRI of mental rotation. Neuroreport 8:3697–3702

Rosen BR, Belliveau JW, Chien D (1989) Perfusion imaging by nuclear magnetic resonance. Magn Reson Q 5:263–281

Rosen BR, Buckner RL, Dale AM (1998) Event-related functional MRI: past, present, future. Proc Natl Acad Sci USA 95:773–780

Saad ZS, Ropella KM, Carman GJ, DeYoe EA (1996) Temporal phase variation of FMR signals in vasculature versus parenchyma. In: Proc ISMRM 4th Annu Meeting, New York

Sakai K, Hikosaka O, Miyauchi S, Takino R, Sasaki Y, Putz B (1998) Transition of brain activation from frontal to parietal areas in visuomotor sequence learning. J Neurosci 18:1827–1840

Savoy RL, O'Craven KM, Weisskoff RM, Davis TL, Baker J, Rosen B (1994) Exploring the temporal bourdaries of fMRI: measuring responses to very brief visual stimuli. In: Book of Abstracts, Soc Neurosci 24th Annu Meeting, Miami

Savoy RL, Bandettini PA, Weisskoff RM, Kwong KK, Davis TL, Baker JR et al. (1995) Pushing the temporal resolution of fMRI: studies of very brief visual stimuli, onset variablity and asynchrony, and stimulus-correlated changes in noise. In: Proc SMR 3rd Annu Meeting, Nice, p.450

Schacter DL, Buckner RL (1998) Priming and the brain. Neuron 20:185–195

Schacter DL, Buckner RL, Koutstaal W, Dale AM, Rosen BR (1997) Late onset of anterior prefrontal activity during true and false recognition: an event related fMRI study. Neuroimage 6:259–269

Schmitt F, Stehling MK, Turner R (1998) Echo-planar imaging: theory, technique, and application. Springer, Berlin Heidelberg New York

Song AW, Wong EC, Tan SG, Hyde JS (1996) Diffusion weighted fMRI at 1.5 T. Magn Reson Med 35:155–158

Stehling MK, Turner R, Mansfield P (1991) Echo-planar imaging: magnetic resonance imaging in a fraction of a second. Science 254:43–50

Turner R, LeBihan D, Moonen CTW, Despres D, Frank J (1991) Echo-planar time course MRI of cat brain oxygenation changes. Magn Reson Med 22:159–166

van Zijl PCM, Eleff SM, Ulatowski JA, Oja JME, Ulug AM, Traystman RJ, Kauppinen RA (1998) Quantitative assessment of blood flow, blood volume and blood oxygenation effects in functional magnetic resonance imagning. Nature Med 4:159–167

Vasquez A, Noll D (1998) Nonlinear aspects of the BOLD response in functional MRI. Neuroimage 7:108–118

Williams DS, Detre JA, Leigh JS, Koretsky AS (1992) Magnetic resonance imaging of perfuusion using spin-inversion of arterial water. Proc Natl Acad Sci USA 89:212–216

Wong EC, Buxton RB, Frank LR (1997) Implementation of quantitative perfusion imaging techniques for functional brain mapping using pulsed arterial spin labeling. NMR Biomed 10:237–249

Wong EC, Buxton RB, Frank LR (1998) Quantitative imaging of perfusion using a single subtraction (QUIPSS and QUIPSSII). Magn Reson Med 39:702–708

Ye FQ, Smith AM, Yang Y, Duyn J, Mattay VS, Ruttimann UE et al. (1997) Quantitation of regional cerebral blood flow increases during motor activation: a steady-state arterial spin tagging study. Neuroimage 6:104–112

Zarahn E, Aguirre G, D'Esposito M (1997) A trial-based experimental design for fMRI. Neuroimage 6:122–138